Journal of Computer-Aided Molecular Design, **15:** 1119–1136, 2002.
KLUWER/ESCOM

Design and synthesis of type-III mimetics of ω-conotoxin GVIA

Jonathan B. Baell[a,*], Stewart A. Forsyth[a], Robert W. Gable[b], Raymond S. Norton[a] & Roger J. Mulder[c]
[a]*Biomolecular Research Institute, 343 Royal Parade, Parkville, Victoria, 3052, Australia;*
[b]*School of Chemistry, University of Melbourne, Parkville, Victoria, 3052, Australia;*
[c]*CSIRO Molecular Science, Bayview Avenue, Clayton, Victoria, 3168, Australia*

Received 19 March 2001; accepted 29 January 2002

Key words: ω-Conotoxin GVIA, ion channel blockers, mimetics, N-type calcium channel, peptidomimetics, proteinomimetics

Summary

Our interest lies in the rational design and synthesis of type-III mimetics of protein and polypeptide structure and function. Our approach involves interactive design of conformationally defined molecular scaffolds that project certain functional groups in a way that mimics the projection of important binding residues as determined in the parent structure. These design principles are discussed and applied to the structurally defined polypeptide, ω-conotoxin GVIA, which blocks voltage-gated, neuronal N-type calcium channels. These ion channels represent therapeutic targets for the development of new analgesics that can treat chronic pain. It is shown how a discontinuous, 3-residue pharmacophore of GVIA can be mimicked by different molecular scaffolds. It is illustrated how such 1st generation leads must necessarily be weak and that optimisability must therefore be built-in during the design process.

Abbreviations: GVIA – ω-Conotoxin GVIA.

Introduction

Peptidomimetic research is a continuously expanding endeavour in the field of drug discovery. In an attempt to classify the diversity of research outcomes from this work, Ripke and Rich [1] defined type-I, type-II and type-III mimetics. Type-I mimetics often match the peptide backbone atom-for-atom, while retaining functionality that makes important contacts with binding sites. Type-II mimetics are nonpeptidic functional mimetics which need not bind to the same site as the endogenous molecule. Type-III mimetics possess novel templates which position important mimetic binding groups appropriately for binding so that they are topographical mimics of the parent peptide even though they may be entirely nonpeptidic.

The potential for drug-likeness makes nonpeptidic type-III mimetics highly attractive from a therapeutic viewpoint, and structurally defined binding epitopes consisting of a few residues of critical importance make attractive targets for the rational design of type-III mimetics. An obvious approach to mimicking such binding epitopes in a nonpeptide is to identify molecular scaffolds that project important sidechain residues appropriately for binding. This is a deceptively difficult task, however, particularly for highly discontinuous binding epitopes where neither backbone connectivity nor secondary structure can be used to guide the design process. This represents a significant challenge as it is increasingly apparent that these sorts of binding epitopes are prevalent in polypeptide- and protein-protein interfaces, which would otherwise

*To whom correspondence should be addressed. E-mail: jbaell@wehi.edu.au
Current addresses:
J.B.B., A.J.H. and R.S.N.: The Walter and Eliza Hall Institute of Medical Research, Post Office of the Royal Melbourne Hospital, Parkville, Victoria, Australia 3050.
S.A.F.: School of Chemistry, Monash University, Clayton, Victoria, Australia.

be attractive prospects for small molecule intervention by rationally designed type-III mimetics [2].

While some attempts have been made at interactive design of nonpeptide, type-III mimetics of such discontinuous pharmacophores, the results have been somewhat ad hoc, mainly because of the difficulty in combining synthetic, conformational and physicochemical aspects of molecules during in silico construction [3–5]. The problem of scaffold *synthesis* can be alleviated by computer-aided searching of databases of available compounds that match target pharmacophores. While this has met with some success in the discovery of nonpeptide, type III mimetics of discontinuous pharmacophores, database diversity limits the generic potential of this approach [6]. The problem of scaffold *conformation* is also suited to automation, particularly of the sort exemplified by Bartlett's CAVEAT vector matching program [7], but the fields of diversity, synthesis, conformation, and physicochemistry again pose difficulties for the use of this technology in the efficient discovery of drug-like, nonpeptidic type-III mimetics. Rather, successes in the use of CAVEAT tend to be limited to inherently much simpler problems [8].

In this paper, we describe our attempts to interactively design and synthesize nonpeptide type III mimetics of ω-conotoxin GVIA, a structurally-defined 27-residue polypeptide isolated from the venom of the fish-hunting cone shell *Conus geographus* [9–11]. GVIA blocks neuronal voltage-gated N-type calcium channels and in doing so has been identified as a potential therapeutic for the relief of chronic pain [12]. While GVIA mimetics could therefore give rise to therapeutically useful compounds, our primary interest here is to investigate the nature of scaffold design and construction, and to experimentally verify that synthesisable, conformationally appropriate scaffolds can be discovered efficiently through interactive design.

Results and discussion

Design and synthesis of scaffolds

GVIA is structurally defined by virtue of a cystine knot [9]. Sidechains responsible for binding to the N-type calcium channel have been previously characterized [10–12] through alanine scanning (Table 1). Important residues include K2 and Y13 (red), and to a lesser extent R17, Y22 and K24 (yellow) (Figure 1), though all residues bar Y13 are relatively weak in their interaction with the N-type calcium channel. The questions arise of how many residues should we attempt to mimic and which should they be? It was felt that a two-sidechain mimetic would be insufficient to register measurable biological activity, and that design and synthetic complexity involved in a four-residue mimetic would be so great as to render the task impractical. Rather, in a generic sense, a three-sidechain mimetic was seen to be the most appropriate. However, while K2 and Y13 were obvious inclusions for a 3 point mimic, it was not clear what the third sidechain mimetic should be – R17, Y22 or K24. All three are quite distant from either K2 and Y13, which are also quite distant from each other, so any of the K2-Y13-R17, K2-Y13-Y22 or K2-Y13-K24 pharmacophores represent a disparate, discontinuous binding epitope. While K24 appears to be functionally more important than either R17 or Y22, more binding energy appears to be attributable to R17. Indeed, replacement of Y22 with alanine gives rise to an *increase* in binding affinity (Table 1). On the other hand, a K2-Y13-Y22 mimetic would have very different physicochemical properties from a K2-Y13-R17 or K2- Y13-K24 mimetic. The former might have more chance of being bioavailable, but the latter two could potentially be delivered as a prodrug and be released irreversibly as a dication in the CNS, thereby circumventing potentially problematic peripherally-mediated hypotensive side-effects [12].

To help resolve this issue, a scaffold that might adequately mimic K2-Y13 was initially sought. The backbone conformation is better defined than the sidechain conformation, and for many residues it is quite uncertain where the sidechain termini might be placed in the bound farm. For this reason, scaffolds which *projected* sidechains appropriately through mimicry of the αC-βC bond vector were concentrated on. In Figure 1(b) it is clear that the αC-βC bond of K2 projects inwardly relative to the plane of any scaffold that might be designed to intervene between it and Y13. This is a good example of how the versatility of peptide conformation can make the mimetic problem superficially more difficult. However, this was envisaged to resemble the geometrical relationship that an ortho-substituent on a phenyl ring attached to a planar structure could have relative to a distal substituent on that planar structure. Iterative interactive design led to the choice of a 6-substituted, 2-(2-substituted-benzamido)benzothiazole system, **1**, shown in Figure 2(a), as a suitable scaffold for mimicry of the K2 and Y13 αC-βC bond vectors. This two-point mimetic

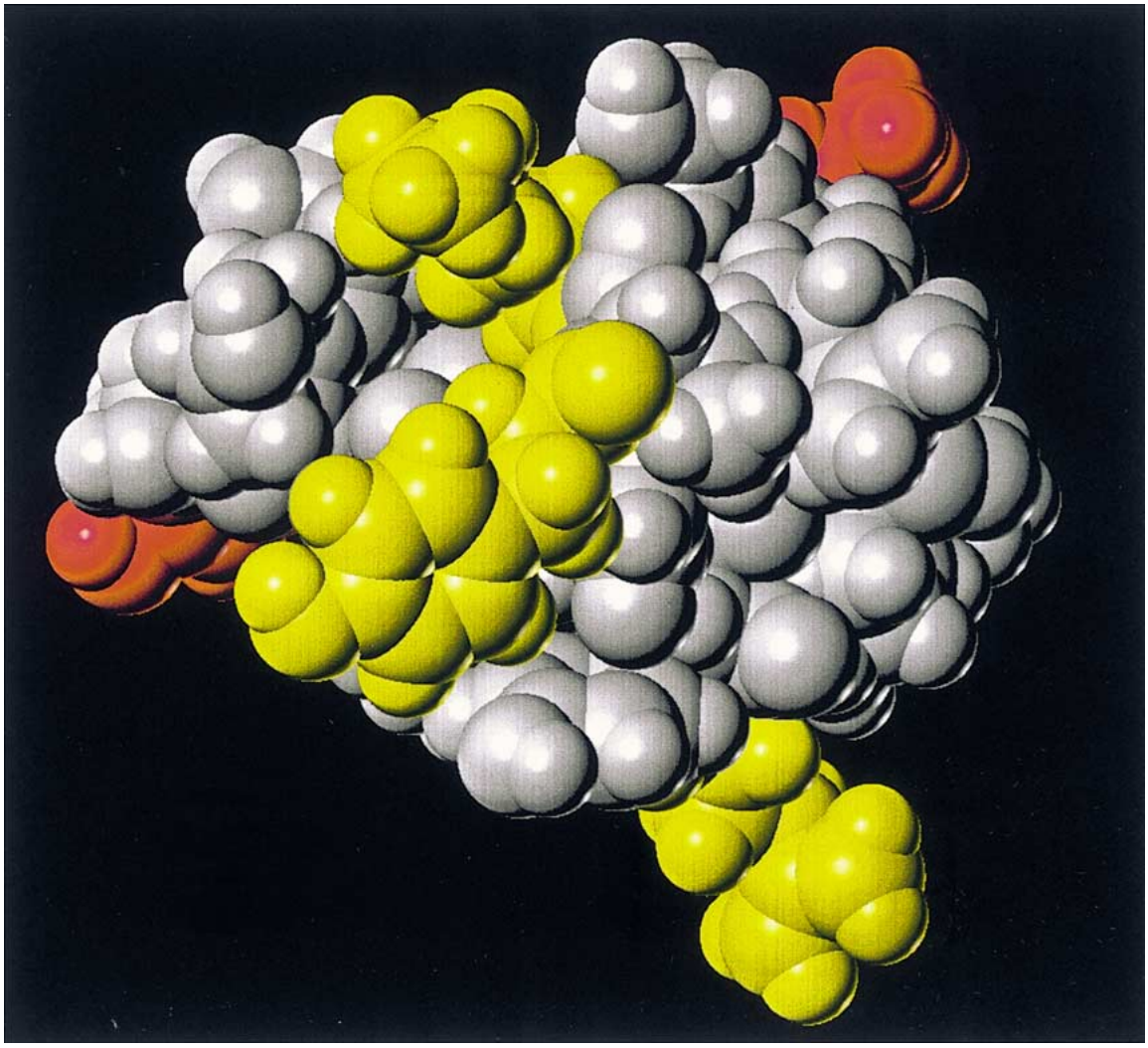

Figure 1. (a) Solution structure of ω-conotoxin GVIA. The most important residues for binding to the N-type calcium channel are K2 and Y13 (coloured red) and less important residues include R17, Y22 and K24 (all coloured yellow). The spatial disposition of these five residues and the α-β bond orientation (purple) are shown more clearly in (b). This same orientation is used in all figures.

was superimposed on the GVIA pharmacophore. Not only was the fit excellent, but it became obvious that N-benzylation would give rise to a pendant benzyl group which would be in the region of the αC-βC bond of R17 (Figure 2(d)). For this reason, R17 was chosen over Y22 as the third residue to be mimicked for the purposes of initial proof-of-concept. Subsequently, mimetic **2**, shown in Figure 2(b) was identified as a putative synthetic target. From physicochemical, stability and synthetic viewpoints, we anticipated that mimetic **2** and the benzothiazole scaffold contained therein would be highly suitable as a type-III mimetic.

Common sense dictates that the benzyl group in **2** could be perpendicular to the plane of the benzothiazole-amide system in either a 'pendant', or an 'erect' sense (Figure 3). MMFF94s as implemented in SYBYL 6.5 [13] was used to estimate the relative net energies involved and it was found that the erect farm was predicted to be more stable than the desired, pendant farm, but by only 5.0 kJ/mol [14, 15]. This was the case regardless of the nature of the substituents in the benzothiazole or benzyl rings. Since this scaffold was not represented in the Cambridge Crystallographic Data Files, the derivative **4** shown in Figure 4(a) was synthesized and analyzed by X-ray crystallography. Its crystal structure (carbon atoms coloured green) is shown in Figure 4(b) superimposed with the two, theoretically-derived con-

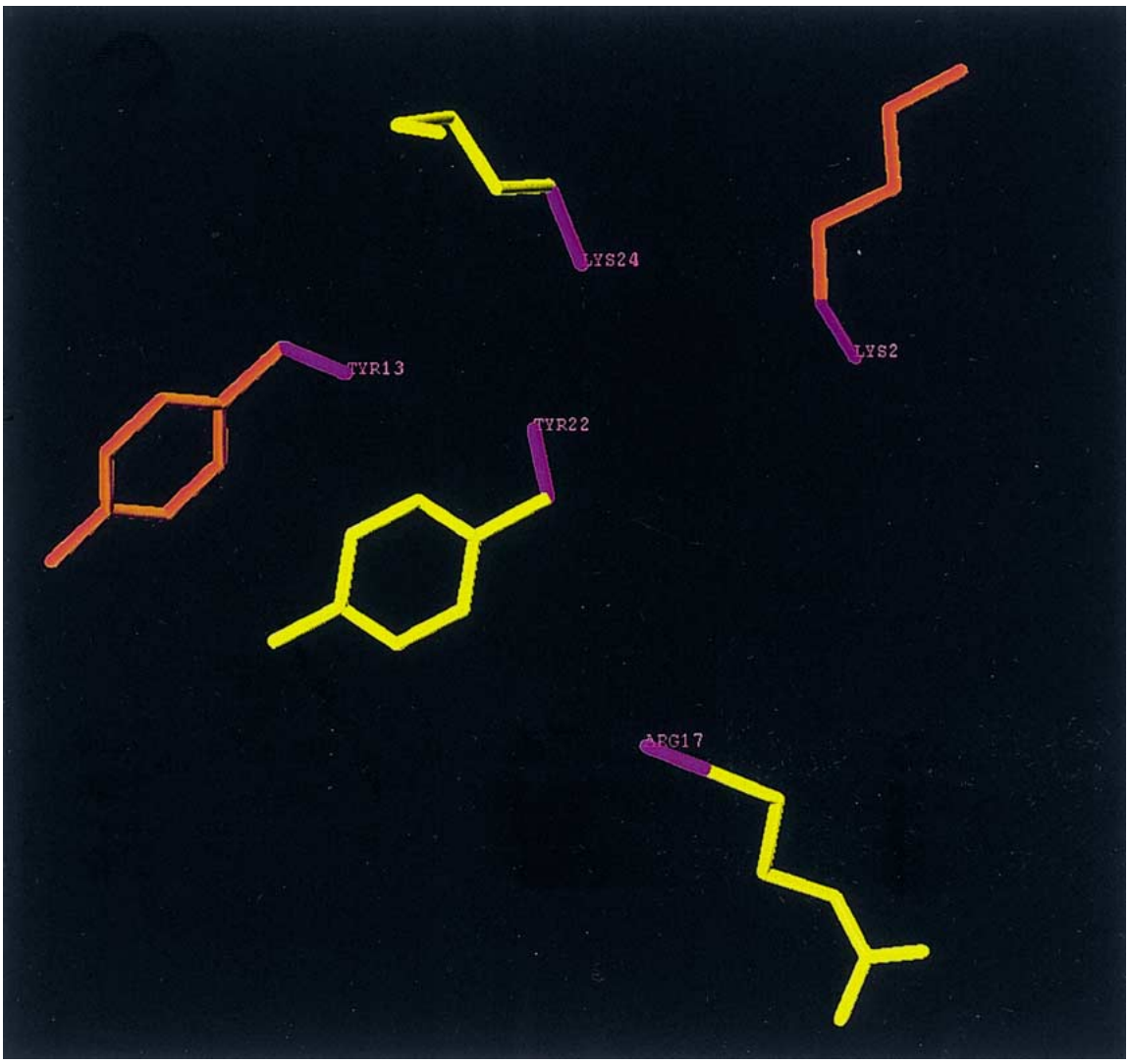

Figure 1. Continued.

formations with pendant and erect benzyl groups. As anticipated, there was coincidence in the solid-state and theoretical farms with respect to the benzyl group in the erect position and being synplanar with the ethoxyphenyl ring, which was twisted ca 90° to the plane of the amide group. One minor difference was that the benzyl phenyl ring was in an eclipsed conformation in the solid state, whereas MMFF94s minimized this to one of the two possible gauche farms, regardless of whether the benzyl group was erect or pendant. In the superimpositions in Figure 2(d) are shown the two gauche conformations and also the eclipsed conformation of the pendant benzyl group.

It was observed in the ^{1}H NMR spectrum of **4** that the methylene protons of the benzyl group gave rise to very broad signals at room temperature in $CDCl_3$ but resolved to a symmetrical pair of doublets on cooling to 260 K (Figure 5). This could be due to a dynamic equilibrium between two mirror images, which presumably could be either the pair where the nitro and ethoxy substituents are on the same side of the amide plane as one another, one of which would correspond to the solid-state structure, or the pair where these respective groups are on the opposite side of the amide plane to one another, one of these corresponding to the desired, pendant benzyl form. This issue was resolved by the observation that while an NOE was observed

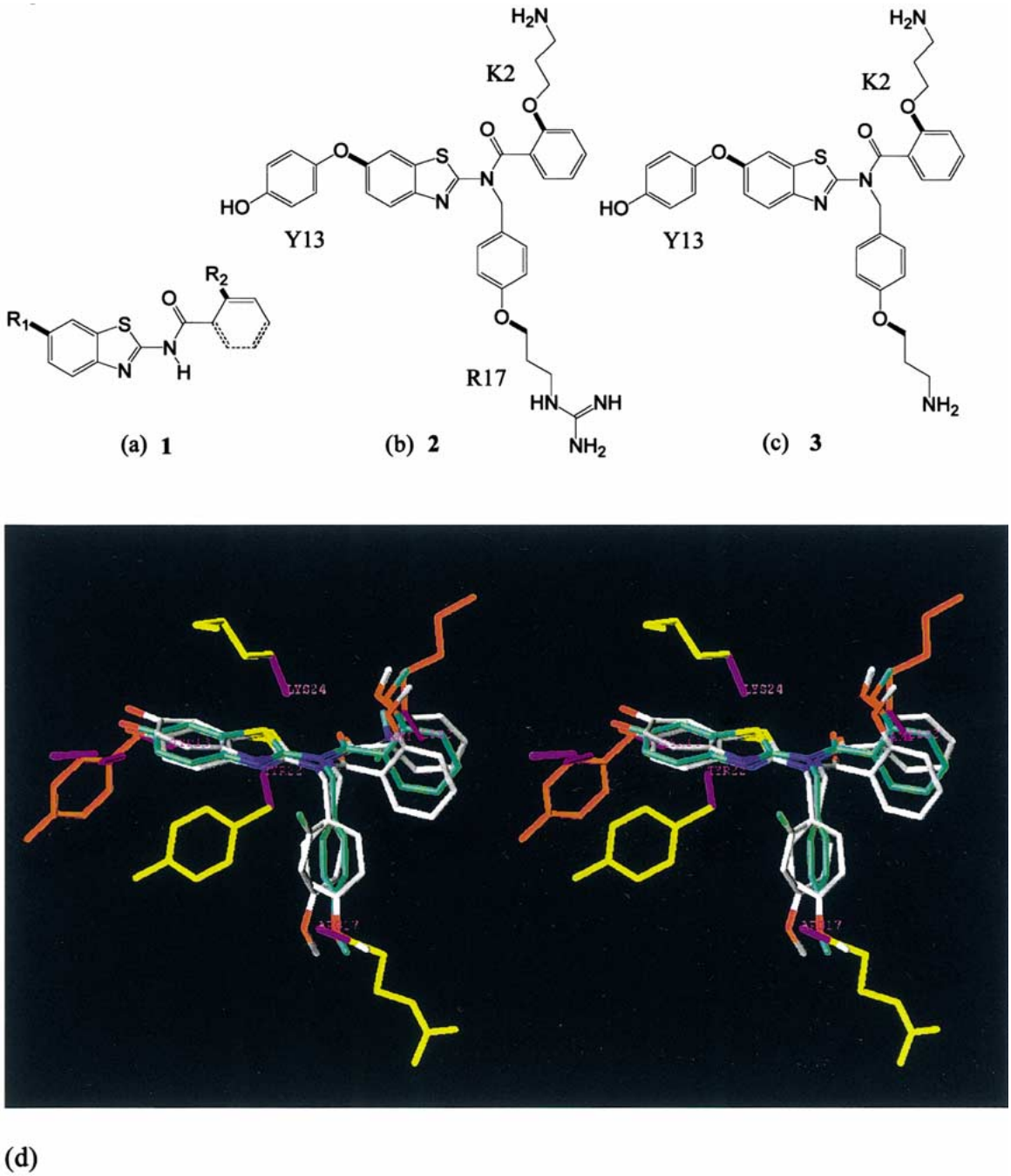

Figure 2. (a) Benzothiazole *1* projects bonds (bold faced) which were anticipated to resemble the relative α-β bond orientation of K2 and Y13 in GVIA. Modelling of **1** suggested N-benzylation as a means to extend mimicry to include R17, giving rise to target mimetic **2** shown in (b). The superimposition of **2** in its desired mimetic conformation – a local minimum predicted by MMF94s – on GVIA is shown in (d) as a relaxed stereoview. Two theoretical local minima are coloured by atom type, whereas the pendant benzyl in the eclipsed conformation, which is found in the solid state, is coloured in light blue. Near Y13 are shown the α-β bonds of GVIA residues 10 (hydroxyproline, in front) and 11 (threonine, behind), which could be mimicked by an appropriately developed derivative of **2** to further increase activity, since there is evidence of binding sites for Arg and Leu respectively at these positions [5, 11]. Analogous comments apply to the GVIA N-terminus, which is shown to be near the amide carbonyl group of **2** and which may contribute to binding to the N-type calcium channel [11]. In one of the theoretical structures, a benzyl aryl proton is displayed, exemplifying a putative linkage point to a more distant Y22-K24 dipeptide mimetic. Compound **3** in (c) is shown because this was found to be inactive, and this result was used to add support to the notion that all groups in **2** were interacting with the N-type calcium channel.

Table 1. Potency loss ratios for inhibition of stimulated rat vas deferens and rat brain binding loss ratios for ω-conotoxin GVIA analogs with respect to blocking N-type calcium channels.

Analogue	Potency loss ratio[a] (no. of determinations)	Binding loss ratio[b]	Decrease in free energy of binding, $\Delta\Delta G_{obs}$ (kJ/mol[c]
K2A	24 (4)	40	8
Y13A	5400 (4)	320	13
R17A	3.9 (3)	6	4
Y22A	3.7 (3)	0.25	−3
K24A	5.7 (4)	2.5	2

[a]Relative to native ω-conotoxin GVIA for ability inhibit stimulated rat vas deferens. Data taken from Flinn *et al.* [11].
[b]Relative to native ω-conotoxin GVIA for ability to bind to rat brain membrane. Data taken from Lew *et al.* [10] using ΔpEC_{50} values of 1.6, 2.5, 0.8, −0.6 and 0.4 respectively.
[c]$\Delta\Delta G_{obs}$ = TRlnK = 230lnK (at 277K, the temperature at which the binding experiments were conducted), where K here is the binding loss ratio.

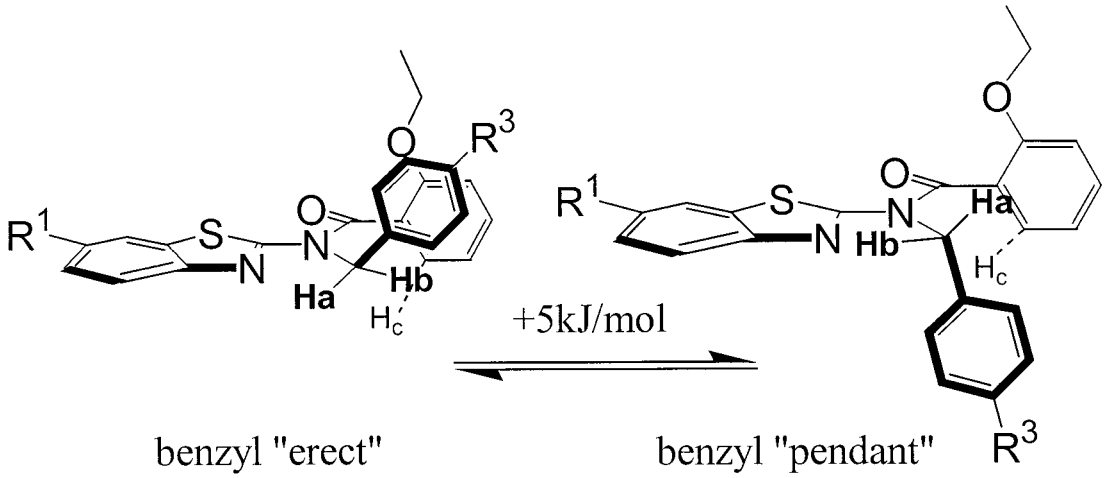

Figure 3. MMF94s predicts the benzyl group in molecules of the type **2** to be 'erect' and synplanar with the nearby alkoxyphenyl ring, although the desired mimetic conformation with the benzyl group 'pendant' is estimated to be only 5 kJ/mol higher in energy. MMF94s incorrectly edicts the benzothiazole sulfur atom to prefer energetically to lie antiperiplanar to the carbonyl group, as illustrated by the benzothiazole 'flipped' form.

between H_a and H_c, and H_b and H_c as defined in Figure 3, none was observed between the ethoxy protons and the aromatic protons ortho to the nitro substituent in the benzyl ring. This is more consistent with the existence of the desired pendant benzyl conformation (and its mirror image) than the solid-state erect benzyl conformation (and its mirror image), and is an example of where solid-state packing forces and solvent molecules work in opposite ways to stabilize different conformations.

On the basis of this analysis, it was decided that **2** was worthy of synthesis. However, as a test of the generic potential for interactive design, it was deemed useful to investigate whether other scaffolds unrelated to **2** could be designed. To be able do so could be useful for a number reasons. For example, the salicylyl ring of the K2 sidechain mimetic in **2** presents a hydrophobic surface which slightly protrudes from the polar surface of GVIA (see Figure 2(d)) and this could be detrimental to biological activity if it interfered with the channel surface which may be nearby. Also, the K2 αC-βC mimetic bond is subject to hindered rotation and this may distort the conformational space able to be sampled by the terminal sidechain nitrogen

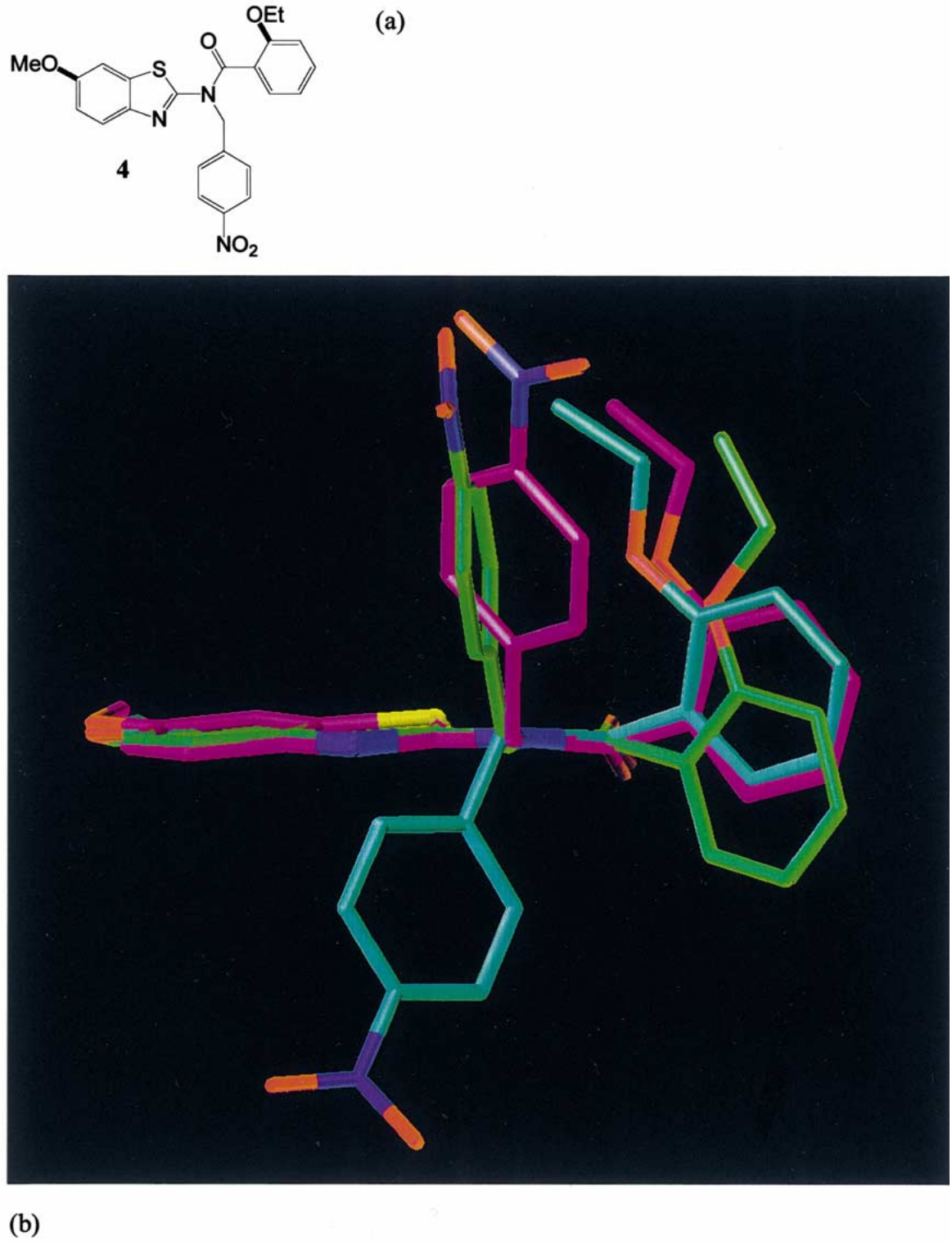

Figure 4. (a) Benzothiazole **4** was chosen as a suitable representative of scaffold conformation in target mimetic **2**. Its crystal structure illustrating the concept of the 'erect' benzyl group is shown in (b) (carbons coloured green), with two MMF94s- predicted local minima superimposed (carbons coloured magenta for an erect benzyl form, and light blue for the pendant benzyl farm). The solid state structure has significant curvature of the amide bond, causing the ethoxyphenyl group to move 'down' relative to the MMF94s-minimized conformer (carbons coloured magenta). The MMF94s conformers prefer a 'gauche' benzyl group over the solid-state eclipsed form. The desired mimetic form is that which coloured light blue.

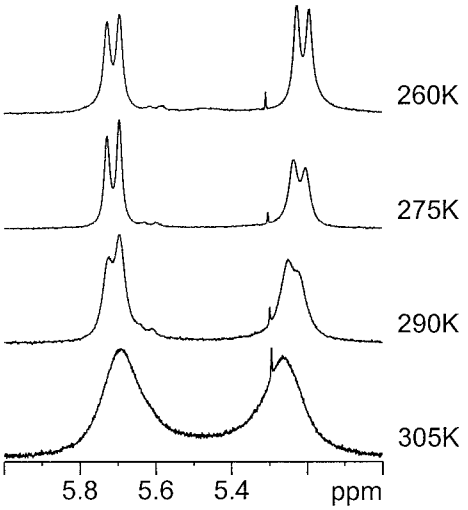

Figure 5. Variable temperature ^{1}H NMR experiments (500 MHz) performed on **4** in $CDCl_3$, illustrating the sharpening of signals corresponding to Ha and Hb in Figure 3 as the temperature lowers, indicative of the freezing out of mirror image conformers. From nOe data, it is inferred that these two mirror image conformers represent the pendant benzyl form (and its mirror image) as drawn in Figure 3 and coloured light blue in Figure 4(b), which also represents the desired mimetic conformation.

atom in mimetic **2**. A different scaffold design could change these properties. Figure 6(a) shows the result of a new interactive design effort with mimetic **5**, which, like mimetic **2**, was embedded with anticipated favourable physicochemical, synthetic, and stability properties during the design process. This anthranilamide derivative has a much looser conformational environment for the K2 mimetic sidechain than its counterpart in mimetic **2** and furthermore, projects a polar carbonyl group in the vicinity of concern where mimetic **2** projects a non-polar aromatic ring. This is more clearly shown in Figure 6(c). There is even less conformational uncertainty in this scaffold than that in mimetic **2**. The intramolecular NH-O=C hydrogen bond dictates the orientation of the outwardly projecting adjoining structures. The only question that remains is the extent to which theoretical and experimental torsions differ in their similarity. As was the case for mimetic **2**, a conformational representative was synthesized and analyzed by X-ray crystallography (Appendix II), shown as **6** in Figure 6(b). The solid state structure was superimposed on the designed structure and as shown in Figure 6(c), there was excellent agreement between the theoretical and experimentally determined conformations. For comparison, mimetic **2** is also shown in blue. Consequently, mimetic **5** was targeted for synthesis but once more,

Table 2. Biological data[a] for GVIA mimetics measured as inhibition to response to sympathetic nerve-mediated contraction of rat vas deferens.[a]

Mimetic	IC_{50} (±20%)
2	98 μM
5	68 μM

[a]Measured in triplicate; ±20%.
[b]Assay performed as described Flinn *et al.* [11].

we wished to test our ability to construct another, unrelated scaffold, which would complement **2** and **5**. For example, while these two scaffolds are different in most ways, they both possess a diphenyl ether group in association with mimicry of Y13, which represents the junction of the mimetic sidechain to the scaffold. For bulky and hindered amino acid sidechains in particular, the αC-βC mimetic approach is potentially limited by undesirable conformational perturbation by the attached scaffold (which may not occur in the native residue), which is a bulky phenyl ring in both mimetics **2** and **5**. Since Y13 is so crucial for biological activity in GVIA and since an inappropriate conformation of this bulky group in the hindered diphenyl ether moiety in mimetics **2** and **5** could therefore result in loss of biological activity, we wanted to loosen the conformational environment of the Y13 mimetic group.

This was achieved by use of an alkyl chain in the interactive design of the imide derivative, mimetic **7** (Figure 7(a)). As was the case for mimetic **5**, there was little conformational choice for the scaffold in mimetic **7** and it was merely a case of how different the theoretical and experimentally-determined torsions were in their similarity. Synthesis and X-ray crystallographic analysis (Appendix III) of a conformational representative of mimetic **7**, namely the simple derivative **8** in Figure 7(b), returned an experimentally derived structure which was in good agreement with that anticipated. The superimposition of the theoretical and experimental structure of the imide scaffold on GVIA is shown in Figure 7(c).

Design and synthesis of functionalised mimetics

Mimetics **2** and **5** were chosen for synthesis. The synthesis of mimetic **7** was set aside as a future project. Synthesis of the target compound **2** was readily achieved convergently in 13 steps (Appendix IV)

Table 3. Distance-constraint matrix (angstroms) for sidechain functional groups[a] in ω-conotoxin GVIA based on NMR data [18] for the purposes of database mining.

	K2	Y13	R17	Y22	K24
K2		13.9 ± 1.6	14.9 ± 2.8	20.2 ± 2.7	16.0 ± 2.7
Y13			15.3 ± 2.4	19.5 ± 1.0	17.0 ± 2.5
R17				18.5 ± 2.9	20.8 ± 2.4
Y22					9.7 ± 1.5
K24					

[a]Distances measured from the terminal nitrogen atom for K2 and K24, the ring centroid for Y13 and Y22, and the trigonal guanidyl carbon atom for R17. For query development, only the terminal NH2 of K2 and K24 was used, the phenol ring of Y13, the phenyl ring of Y22 and the guanidyl group of R17. All three-point queries contained K2 and Y13 with one of the other three residues.

while **5** was readily synthesized convergently in only 8 steps (Appendix V), facilitated in part by the use of the precursor **14**, which was common to the synthesis of mimetic **2**. At the time of testing we had access to only functional and not binding assays, which was a concern since this could return a false negative result. However, despite this potential problem, testing was undertaken in the stimulated rat vas deferens [10, 11] and this returned an IC_{50} of approximately 100 μM and 70 μM for functional blockade of the N-type calcium channel by **2** and **5**, respectively, a result which was considered to represent a successful outcome (Table 2). While it is interesting that mimetic **5** is more potent than mimetic **2**, at this level of biological activity it can only be conjecture as to whether this arises from slightly better structural characteristics, or whether it represents some more efficient transport component in this tissue-based assay.

Do all three mimetic sidechains interact with the N-type calcium channel? To answer this comprehensively requires testing of all possible surrogate sidechain-deleted variants for negative biological activity. While this was not done, we took a precursor of mimetic **2** (compound **17** in Appendix IV) and fully deprotected it to give the benzothiazole derivative **3** in Figure 2(c). This compound was then tested and found to be inactive. That is, the small change on going from a sidechain with a delocalised positive charge to that of a localized positive charge shortened by an Ångstrom or so, abolished activity. This was seen as good evidence that the R17 surrogate contributes to the binding interaction in mimetic **2** and that, taking the two mimetics **2** and **5** together with their similar levels of biological activity, all three residue surrogates are likely to interact with the N-type calcium channel in the manner intended in both mimetics.

Database mining

As a complementary approach, we undertook database-mining, performing pharmacophore searches using the distance constraints of important sidechain functional groups as shown in Table 3, always including the K2 nitrogen atom and the Y13 phenol in the search query with any third residue from R17, Y22 or K24. No hits resulted from searching databases of commercially available compounds [14] – quite simply, the diversity was insufficient. We also used Bartlett's CAVEAT, a software program designed to discover these sorts of type-III mimetics [7]. However, in our hands, we did not discover helpful structures using this technique, or at least, structures which could compete with the quality of those arising from our interactive design efforts.

Conclusions

We have described the successful design of synthesisable, conformationally appropriate 3-residue mimetics of ω-conotoxin GVIA. These are based on the binding epitope as elucidated by alanine-scanning data and NMR spectroscopy. Due to uncertainty in sidechain conformation in the bound farm, efforts were focused on mimicking the αC-βC bond vectors. This represents a general approach for mimicry of polypeptides and proteins whose structure has not been elucidated in complexed form and has three major consequences. Firstly, any 1st generation mimetics discovered are unlikely to exhibit a high degree of activity, especially

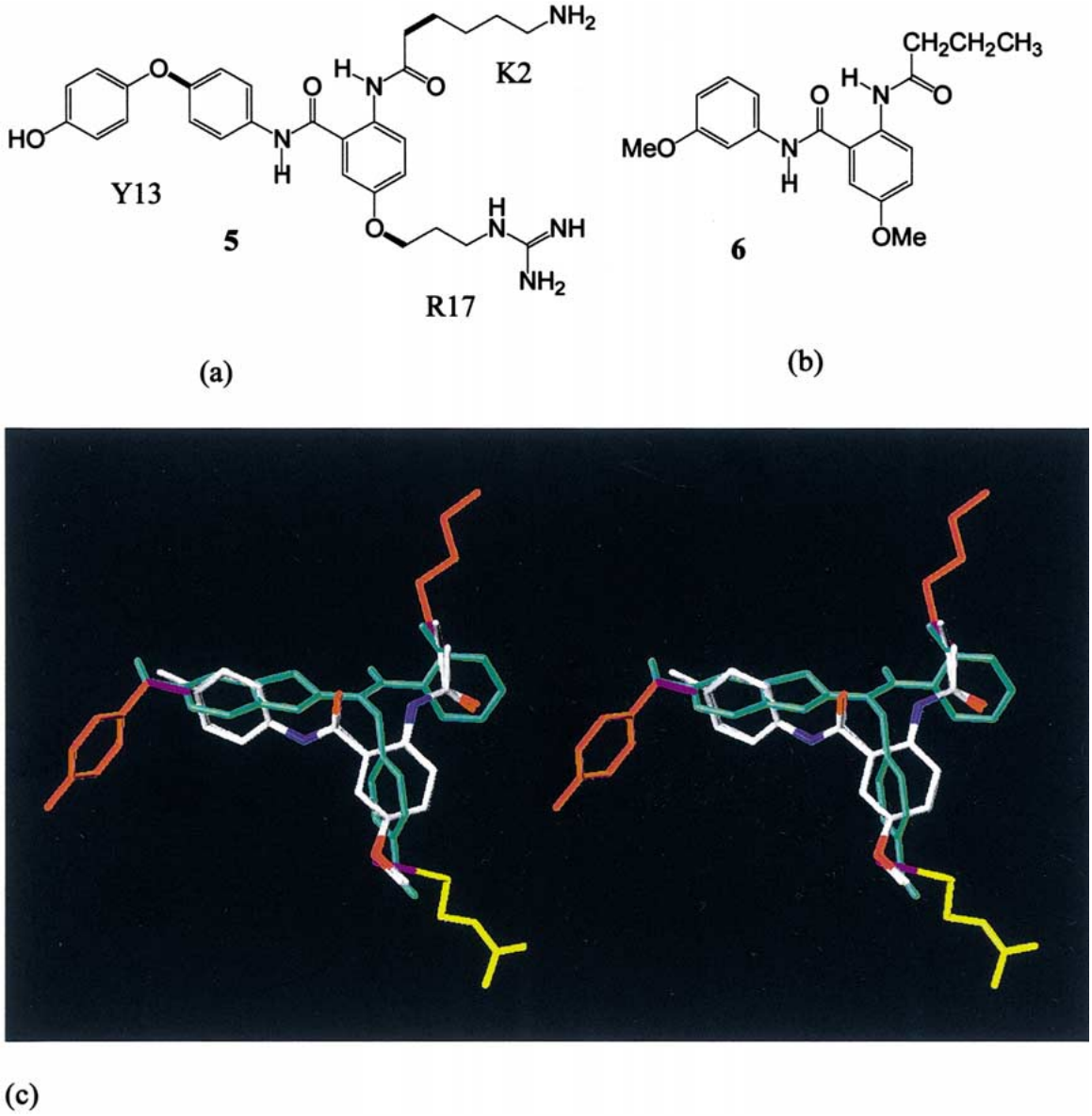

Figure 6. (a) Anthranilamide derivative **5** contains a completely different scaffold to **2** but is predicted to also be a good GVIA K2-Y13-R17 α-β bond mimetic. (b) Simple conformational representative **6** was synthesized and its structure analyzed by X-ray crystallography. (c) Superimposition of the solid-state and theoretical (MMF94s) conformations of the anthranilamide scaffold (coloured by atom type) show almost complete coincidence of atomic coordinates. Superimposed in light blue is shown for comparison the mimetic **2**. This is a relaxed stereoview.

if they contain arginine or lysine mimetic sidechains, which are highly flexible and solvated. Secondly, however, if synthetic junction points are built in between the scaffold and the mimetic sidechain, such compounds become attractive as highly optimisable targets for combinatorial chemistry and multiple parallel synthetic applications. Such is the case for mimetics **2** and **5** disclosed herein, remembering that for binding to be increased by three orders of magnitude, only 17 kJ/mol extra free energy of binding need be found. This could arise from appropriately constraining roughly five of the numerous single bonds present in our mimetics, or additional hydrophobic burying of, for example, a phenyl ring, or a few new hydrogen bonds, or a couple of ionic interactions, or combinations of the above [17]. Thirdly, this stepwise approach allows for some degree of flexing in GVIA since our 1st generation mimetics have a great degree of con-

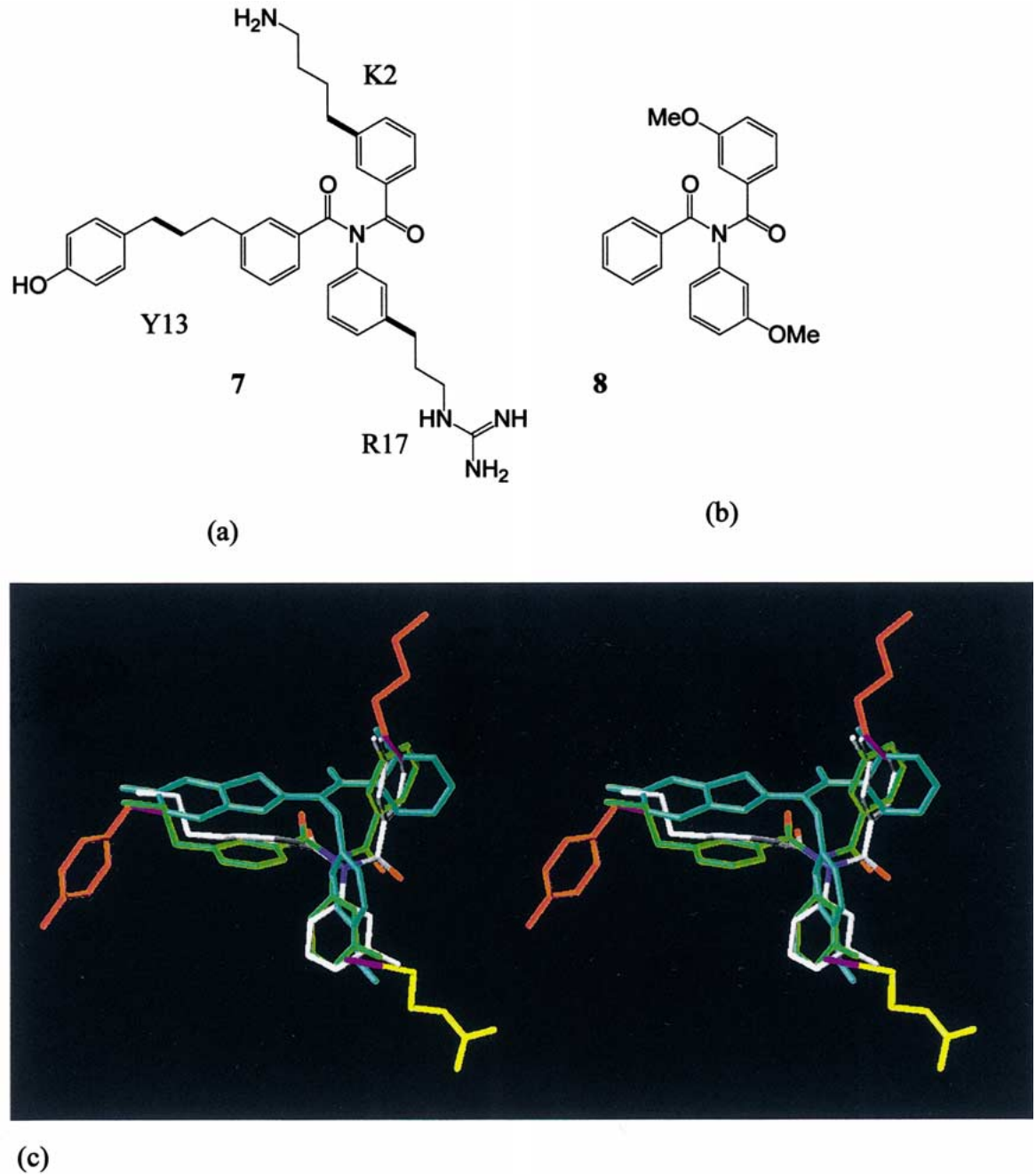

Figure 7. (a) Imide derivative **7** contains a completely different scaffold to **2** and **5** but is predicted to also be a good GVIA K2- Y13-R17 α-β bond mimetic. (b) Simple conformational representative **8** was synthesized and its structure analyzed by X-ray crystallography. (c) Superimposition of the solid-state (coloured green) and theoretical (MMF94s, coloured by atom type) conformations of the imide scaffold show good coincidence of molecular structure. Superimposed in light blue is shown for comparison the mimetic **2**. This is a relaxed stereoview.

formational flexibility in the K2 and R17 mimetic sidechains, which could sample a large amount of conformational space. Indeed, the ω-conotoxins appear to be able to undergo some conformational change in the vicinity of the pharmacophore [18, 19], and it is possible that mimetics **2** and **5** may bind to the K2-Y13-R17 binding site not by emulating the αC-βC bond vectors exactly as envisaged from the solution structure of GVIA. In this sense, 2nd and 3rd generation, conformationally constrained type-III mimetics could be useful not only as therapeutic candidates, but as structural probes to shed light on this issue.

The GVIA pharmacophore targeted is particularly challenging in that it represents a discontinuous, disparate binding epitope, where sidechain conformation is uncertain and whose individual residues apparently bind much more weakly than individual residues in similarly discontinuous binding epitopes described for a number of protein-protein interactions [20–26]. Indeed, protein-protein complexes usually have information on sidechain conformation in the bound form, giving rise to the possibility of designing 1st generation type-III mimetics more constrained than those reported here. It is entirely plausible therefore that relatively potent inhibitors could be discovered in the 1st generation of mimetics of such protein-protein interactions [27, 28]. To date, the discovery of potent type-III mimetic antagonists of protein-protein interactions has generally been restricted to those cases where most of the biological activity is encoded in a short contiguous sequence [29–35]. Here, structural information has often been scarce and an intensive synthetic effort has usually been required to obtain a good outcome, more akin to traditional type-III peptidomimetic development. An elegant exception is the structure-based design of a nonpeptidic alpha-helix mimetic reported recently by the Hamilton group [35], which could be of general use to other complexes involving helix-binding grooves [36, 37]. Here, knowledge of alpha-helical structure was used to aid the design.

A different perspective to structure-based design of nonpeptidic type-III mimetics which has been presented here is the ability of interactive design to efficiently encompass mimicry of highly discontinuous residues where a secondary structural form is not present and which cannot therefore be used to aid design. It is anticipated that future work will report not only on the discovery of 1st generation type-III mimetics of other polypeptides and proteins, but on the optimisation of such leads to therapeutically interesting levels of activity.

Acknowledgements

We gratefully acknowledge the expert biological testing for N-type calcium channel inhibitory activity by James A. Angus, Michael J. Lew and Arthur Christopoulos, from the Department of Pharmacology, University of Melbourne.

Appendices for synthetic schemes

All compounds have been fully characterized by NMR and mass spectroscopy. Full synthetic details will be published in due course. Reaction solvent is given in square brackets, recrystallisation or trituration solvent in curly brackets. Where necessary, reactions were performed under an inert atmosphere. Unless stated otherwise, reactions were performed at room temperature and pressure.

Less common abbreviations are as follows: DAST – diethylaminosulfur trifluoride; DCE – 1,2-dichloroethane; DIPEA – N,N-diisopropyl ethylamine; DME – dimethoxyethane; HBTU – O-(Benzotriazol-1-yl)-N,N ,N',N'-tetramethyluronium hexafluorophosphate; TEA – triethylamine; TFE – 1,1,1-trifluoroethanol.

Appendix I. Synthesis and essential crystal structure details of scaffold **4**.

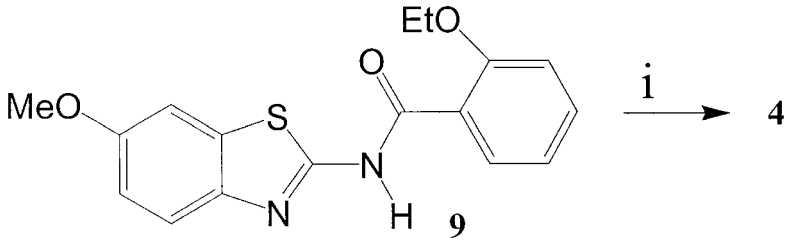

(i) p-NO_2PhCH_2Cl, K_2CO_3, $Bu_4N^+Br^-$ (cat.), 12h [acetone], 83%. Crystals of **4** suitable for x-ray crystallographic analysis were grown from cyclohexane: $C_{24}H_{21}N_3O_5S$, $M = 463.50$, monoclinic, C2/c, $a = 16.7378(14)$, $b = 18.657(2)$, $c = 15.073(3)$ Å, $\beta = 104.497(15)°$, $U = 4557.1(11)$ Å^3, $Z = 8$, $D_{cal} = 1.351$ gcm^{-3}, Cu-Kα radiation, (λ. = 1.5418 Å). 5601 reflections, of which 4705 were unique, were collected on an Enraf-Nonius CAD-4MachS diffractometer using the $\omega : 2\theta$ scan method ($\theta_{max} = 75°$); absorption corrections were applied. The structure was solved by direct methods (SHELXS97) [38] and all non-hydrogen atoms were refined anisotropically; hydrogen atoms were included at geometrical estimates. Full matrix least squares refinement on F_O^2 (SHELXL97) [39] converged with R(F) 0.047 for 3632 reflections [I $> 2\sigma$(I)] $R_W(F^2)$ [all data] 0.138.

Appendix II. Synthesis and essential X-ray crystallographic data for anthranilamide scaffold **6**.

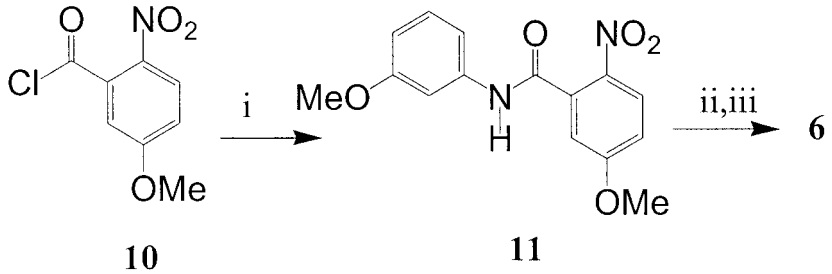

(i) m-anisidine, 2 h [pyridine], 65% {MeOH/water}; (ii) ammonium formate, 10% Pd/C (cat.), 30 min [MeOH], 68%; (iii) butyryl chloride, pyridine, 87%. Crystals of **6** suitable for x-ray crystallographic analysis were grown from DCM/cyclohexane: $C_{19}H_{22}N_2O_4$, $M = 342.39$, triclinic, P^{-1}, $a = 8.0008(6)$, $b = 10.2346(12)$, $c = 12.0706(7)$ Å, $\alpha = 73.454(7)$, $\beta = 76.654(5)$, $\gamma = 74.359(8)°$, $U = 899.59(12)$ Å^3, $Z = 2$, $D_{cal} = 1.264$ gcm^{-3}, Cu-Kα radiation, ($\lambda = 1.5418$ Å). 4333 reflections, of which 3688 were unique, were collected on an Enraf-Nonius CAD-4MachS diffractometer using the $\omega : 2\theta$ scan method ($\theta_{max} = 75°$); absorption corrections were applied. The structure was solved by direct methods (SHELXS97) [38] and all non-hydrogen atoms were refined anisotropically; hydrogen atoms were included in the refinement, except for the methyl hydrogen atoms which were constrained to geometrical estimates. Full matrix least squares refinement on F_O^2 (SHELXL97) [39] converged with R(F) 0.042

for 3422 reflections [I $>$ 2σ(I)] and $R_W(F^2)$ [all data] 0.123.

Appendix III. Synthesis and essential X-ray crystallographic data for imide scaffold **8**.

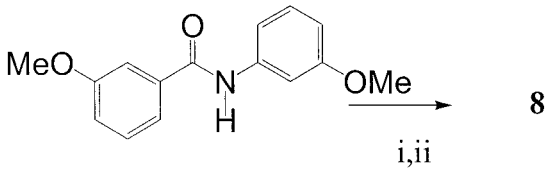

12

(i) NaH, 3h [DMF]; (ii) Benzoyl chloride, 30%. Crystals of **8** suitable for x- ray crystallographic analysis were grown from acetic acid/ether: $C_{22}H_{19}NO_4$, M = 361.38, triclinic, P^{-1}, a = 8.1317(8), b = 8.9485(7), c = 13.5896(6) Å, α = 89.083(5), β = 78.694(6), γ = 71.002(8)°, U = 915.64(12) Å^3, Z = 2, D_{cal} = 1.311 gcm^{-3}, Cu-Kα radiation, (λ = 1.5418 Å). 4594 reflections, of which 3766 were unique, were collected on an Enraf-Nonius CAD-4MachS diffractometer using the ω : 2θ scan method (θ_{max} = 75°); absorption corrections were applied. The structure was solved by direct methods (SHELXS97) [38] and all non-hydrogen atoms were refined anisotropically; hydrogen atoms were included in the refinement, except for the methyl hydrogen atoms which were constrained to geometrical estimates. Full matrix least squares refinement on F_O^2 of (SHELXL97) [39] converged with R(F) 0.037 for 3168 reflections [I $>$ 2σ(I)] and $R_W(F^2)$ [all data] 0.108.

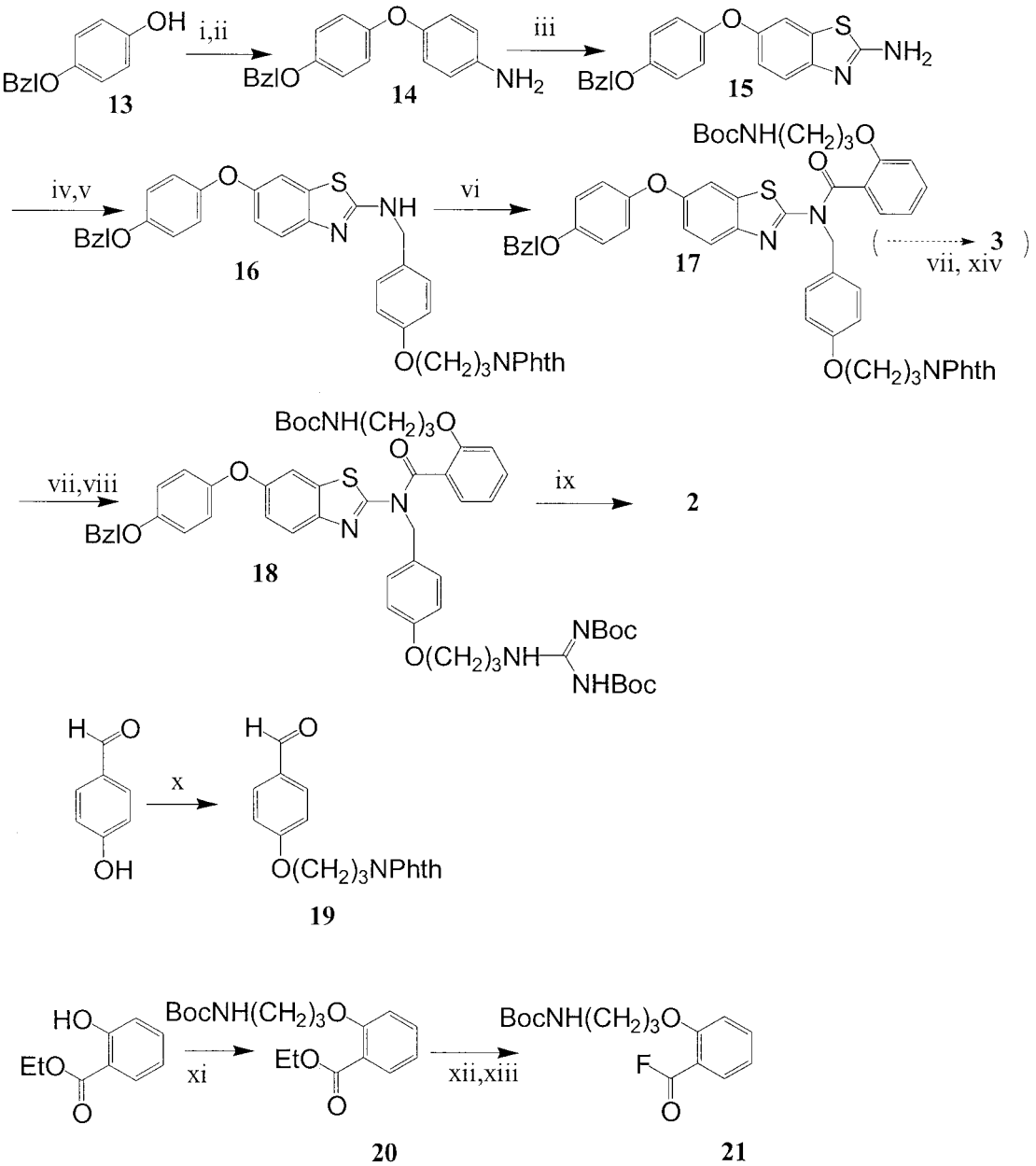

(i) p-NO_2PhNO_2, K_2CO_3, 2h (100 °C) [DMF], 87%; (ii) dithionite reduction, 65%; (iii) KSCN, Br_2, 2h (0 °C), 10h (r.t.) [20% formic/acetic acid], 54%; (iv) **19**, 12h (reflux) [toluene/cyclohexane], 72%; (v) $NaBH_4$ [EtOH], 78%; (vi) **21**, DIPEA, 30min (100 °C) [toluene], 56%; (vii) hydrazine [EtOH]; (viii) $CF_3SO_2N{=}C(NHBoc)_2$, TEA [DCM], 69% over 2 steps; (ix) TFA/thioanisole, 50% after HPLC; (x) $Br(CH_2)_3NPhth$, K_2CO_3, 2h (100 °C) [DMF], 93%; (xi) $Br(CH_2)_3NHBoc$, K_2CO_3, 2h (100 °C) [DMF], 75%; (xii) NaOH, 10h (reflux) [water/ethanol], 80%; (xiii) DAST, 30min (O°C) [DCM], 93%; (xiv) TFA/thioanisole, 31% after HPLC.

Remarks. Synthesis of **2** was facilitated by a number of noteworthy reaction conditions. Firstly, the use of 20% formic acid in acetic acid and resulting freezing point depression enabled the thiocyanation of **14** to give **15** to be performed at close to 0 °C, and this minimized side reactions involving ring bromination. Secondly, the exocyclic amine of **15** was resistant to imine formation and could not be reductively alkylated to **16** in one step. Instead, forcing Dean-Stark conditions were employed to give the bright yellow imine as an intermediate, which was

then reduced by sodium borohydride in dry ethanol to precipitate **16** as a colourless powder. Thirdly, acylation of the poorly reactive benzylamine nitrogen atom in **16** proceeded smoothly using the acid fluoride of the K2 mimetic component, **21** made through the use of DAST as described by the Carpino group [40]. After removal of the phthalimide protecting group in **18**, guanidylation was achieved using the excellent reagent developed by Feichtinger et al. [41] – which synthesis we have improved [42] – followed by deprotection with TFA/thioanisole [43] and HPLC purification.

Appendix V: Synthesis of mimetic **5**.

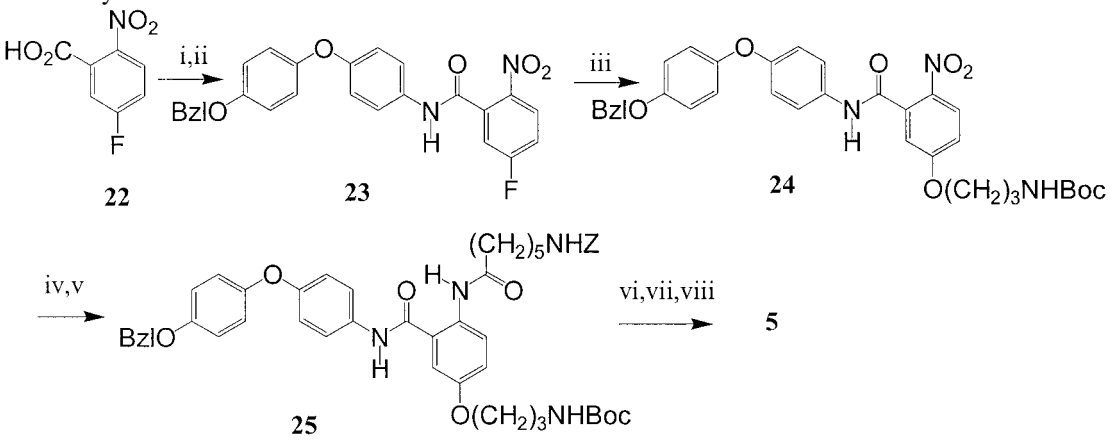

(i) thionyl chloride, 3 h (reflux); (ii) **14**, 10 h [pyridine], 70% toluene; (iii) $HO(CH_2)_3NHBoc$, NaH, 10 h [DME], 55% {MeOH}; (iv) $SnCl_2$, ammonium formate, 3 h (reflux) [MeOH], 60% {ether trituration}; (v) $ZNH(CH_2)_5C(=O)F$, 10 h [pyridine], 60% {MeCN}; (vi) $SnCl_4$, 45 min, [EtOAc/MeCN], 74%; (vii) $CF_3SO_2N{=}C(NHZ)_2$, TEA, [DCM], 72% {DCM/EtOH}; (viii) H_2, 10% Pd/C, 4 h [TFE], 65% {MeOH/Ether}.

Remarks. The synthesis of **5** is noteworthy in a number of ways. Firstly, the smooth displacement of the aryl fluoride in **22**, despite hydride-induced deprotonation of the benzanilide NH, exclusively by the oxygen atom of the di-deprotonated N-BOC-protected alkoxide. Secondly, the use of ammonium formate to buffer the acidity in the reduction of **24**, which can otherwise result in partial loss of the Boc group. Thirdly, activation of Z-protected caproic acid as the acid fluoride using DAST [40], rather than the unstable acid chloride, to give **25**. Fourthly, the use of extremely mild conditions [44] to remove the Boc group in **25**, which otherwise results in the apparent loss of the diphenyl ether moiety.

References

1. Ripka, A.S. and Rich, D.H., Curr. Opin. Chem. Biol., 2 (1998) 441.
2. Kasher, R., Oren, D., Barda, Y. and Gilon C., J. Mol. Biol., 292 (1999) 421 (and references therein).
3. Tilley, J.W., Chen, L., Fry, D.C., Emerson, S.D., Powers, G.D., Biondi, D., Varnell, T., Trilles, R., Guthrie, R., Mennona, F., Kaplan, G., LeMahieu, R.A., Carson, M., Han, R.-J., Liu, C.-M., Palermo, R. and Ju, G., J. Am. Chem. Soc., 119 (1997) 7589.
4. Sarabu, R., Cooper, J.P., Cook, C.M. Gillespie, P., Perrotta, A.V. and Olson, G.L., Drug Des. Discov., 15 (1998) 191.
5. Menzler, S., Bikker, J.A., Suman-Chauhan, N. and Horwell, D.C., Bioorg. Med. Chem. Lett., 10 (2000) 345.
6. Perrier, V., Wallace, A.C., Kaneko, K., Safar, J., Prusiner, S.B. and Cohen, F.E., Proc. Natl. Acad. Sci. USA, 97 (2000) 6073.
7. Lauri, G. and Bartlett, P.A., J. Comput. Aid. Mol. Des., 8 (1994) 51.
8. Yang, W., He, H. and Drueckhammer, D.G., Angew. Chem. Int. Ed., 40 (2001) 1714.
9. Norton, R.S. and Pallaghy, P.K., Toxicon, 36 (1998) 1573.
10. Lew, M.J., Flinn, J.P., Pallaghy, P.K., Murphy, R., Whorlow, S.L., Wright, C.E., Norton, R.S. and Angus, J.A., J. Biol. Chem., 272 (1997) 12014.
11. Flinn, J.P., Pallaghy, P.K., Lew, M.J., Murphy, R., Angus, J.A. and Norton, R.S., Eur. J. Biochem., 262 (1999) 447.
12. Norton, R.S., Pallaghy, P.K., Baell, J.B., Wright, C.E., Lew, M.J. and Angus, J.A., Drug Develop. Res., 46 (1999) 206.
13. Halgren, T.A., J. Comput. Chem., 20 (1999) 720.
14. For all minimizations and forcefield calculations, MMF94s [13] was used as implemented in SYBYL 6.5 (Tripos Associates; http://www.tripos.com), with distance-dependent dielectric ($\varepsilon = 1$). Default settings were used for the minimization process. For investigating known solid-state structures, the Cambridge Crystallographic Data Files were searched using UNITY 4.1 as interfaced to SYBYL 6.5. For searching databases for commercially available compounds, queries were constructed using UNITY 4.1 matches sought for Aldrich(96), Maybridge(98), and an in-house database of more than 100,000 available chemicals. This latter database includes collections derived from Asinex, MDPI, Ost and ChemStar and was converted in 3D format using CONCORD, and into UNITY format using scripts as supplied within SYBYL6.5.
15. In Figure 2(d), the benzothiazole sulfur atom is synplanar with the amide oxygen atom and yet it is estimated by MMFF94s that this is less preferred by 13.0 kj/mol than having the benzothiazole 'flipped' 180° that is, with the endocyclic nitrogen atom synplanar with the amide oxygen atom. This is the case regardless of whether the benzyl group is pendant or erect. The theoretically less-preferred form is maintained in Figure 2(d) because in all of the several examples of N-acylated 2-aminothiazole derivatives present in the Cambridge Crystallographic Data Files, the thiazole sulfur atom is synplanar with the amide oxygen atom and yet MMFF94s consistently estimates the alternative 'flipped' synplanar form as being preferable by 12–22 kj/mol for these molecules. We believe this discrepancy represents forcefield error, and x-ray crystallographic analysis of **4** subsequently supported this assertion. Conveniently, there are certain synthetic advantages in having the Y13 mimetic group substituted in the 6-position as is most appropriate for the sulfur-oxygen synplanar conformation, rather than the 5-position, which would be most appropriate for the alternative form. For example, we envisaged that displacement of a labile para-substituent on a nitrobenzene ring by an appropriately substituted phenoxide group would readily give rise to Y13-mimetic sidechain incorporation in the 6-position of the benzothiazole (see Appendix IV). Also, with a substituent in this position, an alternative and convenient thiocyanation route for the formation of 2-aminobenzothiazoles from anilines is possible, in addition to the classical Hugerschoff synthesis of 2-aminobenzothiazoles via oxidative cyclisation of phenylthioureas [16]. Furthermore, there is the potential to intro duce the Y13 mimetic later in the synthesis as aromatic electrophilic substitution occurs preferentially at the 6-position of 2-aminobenzothiazoles [16].
16. Sprague, J.M. and Land, A.H., in Elderfield, R.C. (ed.), Heterocyclic Compounds, Volume 5, Wiley, New York, 1957, pp. 484–722.
17. Williams, D.H. and Westwell, M.S., Chem. Soc. Rev., 27 (1998) 57.
18. Pallaghy, P.K. and Norton, R.S., J. Pept. Res., 53 (1999) 343.
19. Goldenberg, D.P., Koehn, R.E., Gilbert, D.E. and Wagner, G., Protein Sci., 10 (2001) 538.
20. Vaughan, C.K., Buckle, A.M. and Fersht, A.R., J. Mol. Biol., 286 (1999) 1487.
21. Bogan, A.A. and Thorn, K.S., J. Mol. Biol., 280 (1998) 1.
22. Clackson, T., Ultsch, M.H., Wells, J.A. and de Vos, A.M., J. Mol. Biol., 277 (1998) 1.
23. Shapiro, R., Ruiz-Gutierrez, M. and Chen, C.-Z., J. Mol. Biol., 302 (2000) 497.
24. Kuehlmann, U.C., Pommer, A.J., Moore, G.R., James, R. and Kleanthous, C., J. Mol. Biol., 301 (2000) 1163.
25. Reinemer, P., Sebald, W. and Duschl, A., Angew. Chem. Int. Ed., 39 (2000) 2834.
26. Clackson, T. and Wells, J., Science, 267 (1995) 383.
27. If this is considered an advantage over targeting mimetics of pharmacologically active toxins, it should also be pointed out that the latter have no endogenous partner with which to compete, and which could otherwise place more stringent criteria on the degree of potency required for therapeutic relevance.
28. For a useful review on small molecule inhibitors of protein-protein interactions, see Cochran, A., Chem. Biol., 7 (2000) R85.
29. Plummer, M.S., Holland, D.R., Shahripour, A., Lunney, E.A., Fergus, J.H., Marks, J.S., McConnell, P., Mueller, W.T. and Sawyer T.K., J. Med. Chem., 40 (1997) 3719.
30. Andrade-Gordon P., Maryanoff, B.E., Derian, C.K., Zhang, H.-C., Addo, M.F., Darrow, A.L., Eckardt, A.J., Hoekstra, W.J., McComsey, D.F., Oksenberg, D., Reynolds, E.E., Santulli, R., Scarborough, R.M., Smith, C.E. and White, K.B., Proc. Natl. Acad. Sci. USA, 96 (1999) 12257.
31. Liuzzi, M., Deziel, R., Moss, N., Beaulieu, P., Bonneau, A.-M., Bousquet, C., Chafouleas, J.G., Garneau, M., Jaramillo, J., Krogsrud, R.L., Lagace, L., McCollum, R.S., Nawoot, S. and Guindon, Y., Nature, 372 (1994) 695.
32. Qian, Y., Vogt, A., Vasudevan, A., Sebti, S.M. and Hamilton, A.D., Bioorg. Med. Chem., 6 (1998) 293.
33. Stanfield, R.L. and Wilson, I.A., Curr. Opin. Struct. Biol., 5 (1995) 103.
34. Sulyok, G.A.G., Gibson, C., Goodman, S.L., Hoelzemann, G., Wiesner, M. and Kessler, H., J. Med. Chem., 44 (2001) 1938.
35. Orner, B.P., Ernst, J.T. and Hamilton, A.D., J. Am. Chem. Soc., 123 (2001) 5382.
36. Scanlon, M.J., Fairlie, D.P., Craik, D.J., Englebretsen, D.R. and West, M.L., Biochem., 34 (1995) 8242.

37. Petros, A.M., Nettesheim, D.G., Wang, Y., Olejniczak, E.T., Meadows, R.P., Mack, J., Swift, K., Matayoshi, E.D., Zhang, H., Thompson, C.B. and Fesik, S.W., Protein Sci., 9 (2000) 2528.
38. Sheldrick, G.M., 'SHELXS-97'. Program for crystal structure solution, University of Goettingen, Germany (1997).
39. Sheldrick, G.M., 'SHELXL-97'. Program for crystal structure refinement, University of Goettingen, Germany (1997).
40. Kaduk, C., Wenschuh, H., Beyermann, M., Forner, K., Carpino, L. and Bienert, M., Lett. Pept. Sci., 2 (1995) 285.
41. Feichtinger, K., Sings, H.L., Baker, T.J., Matthews, K. and Goodman, M., J. Org. Chem., 63 (1998) 8432.
42. We found that ethylene diamine (2 eq. in MeOH, minutes) converted the tris(boc)guanidyl by-product to the desired bis(boc) guanidyl precursor.
43. Kiso, Y., Ukawa, K., Nakamura, S., Ito, K. and Akita, T., Chem. Pharm. Bull., 28 (1980) 673.
44. Miel, H. and Rault, S., Tetrahedron Lett., 38 (1997) 7865. No mention is made of problematic tin salts in workup (if product fails to crystallise), which we found best dealt with by use of aqueous sodium potassium tartrate.